

Analysis of Unbalanced Response of Rigid Rotor Supported by AMBs under Coupling Dynamic and Control Methods

Guowei Du^{1,2,3}, Zhengang Shi^{1,2,3}, Haoyu Zuo^{1,2,3}, Lei Zhao^{1,2,3}, and Zhe Sun^{*1,2,3}

¹Institute of Nuclear and New Energy Technology

²Collaborative Innovation Center of Advanced Nuclear Energy Technology

³The Key Laboratory of Advanced Reactor Engineering and Safety
dgw13@mails.tsinghua.edu.cn, sun_zhe@mail.tsinghua.edu.cn*

Abstract — The main helium circulator is the core component of the High Temperature Reactor (HTR). Mechanical machining errors and assembly errors can cause uneven distribution of rotor mass. When the rotor rotates, the unbalanced mass will generate unbalanced force which will change the rotor's axis trajectory. By coupling the rotor dynamics method and the electromagnetic bearing system control theory, the motion of the rotor is modeled. Three representative unbalanced conditions of the impeller position, the bearing position and the centroid position are assumed to simulate the unbalance response of the rotor, and the influence of changes in the stiffness and damping on the unbalance response of the rotor is analyzed by adjusting the stiffness and the damping of the rotor. The results of the analysis show that the bearings farther from the unbalanced position (UBP) have larger rotor displacements and bearing loads. Increasing Active Magnetic Bearings (AMBs) stiffness and damping will increase the bearing load and reduce the response displacement of the rotor. Therefore, the stiffness and damping of AMBs must be designed by considering the bearing capacity and the displacement limit of the rotor.

Index Terms — Active magnetic bearing, bearing stiffness and damping, coupling dynamic and control methods, rigid rotor, unbalance response.

I. MODEL INTRODUCTION

A. The rotor model

The main helium circulator model of the HTR is shown in Fig. 1. The vertical rotor (red part) is supported by two radial electromagnetic bearings (yellow sections). Because the first-order bending frequency of the rotor exceeds the rated rotation speed of the rotor, the rotor is simplified as a rigid rotor and placed in a rectangular coordinate system, as shown in Fig. 2, the dynamic parameters of the rotor are shown in Table 1.

In Fig. 2, The notation x_a represents the rotor displacement in the x direction at bearing A, the notation y_a represents the rotor displacement in the y direction at

bearing A, and the notation F_{xa} represents the bearing force applied to the rotor by the bearing A in the x direction, the notation F_{ya} represents the bearing force applied to the rotor by the bearing A in the y direction, as is the case for the bearing B. The notation x_c represents the displacement of the centroid in the x direction, notation y_c represents the displacement of the centroid in the y direction, and the notation θ_x represents the rotation angle of the rotor around the x axis, the notation θ_y represents the rotation angle of the rotor around the y axis. The notation P represents the external load, the notation C represents the centroid, the notation l represents the force arm of the force from the centroid, and the notation Ω represents the rotational speed.

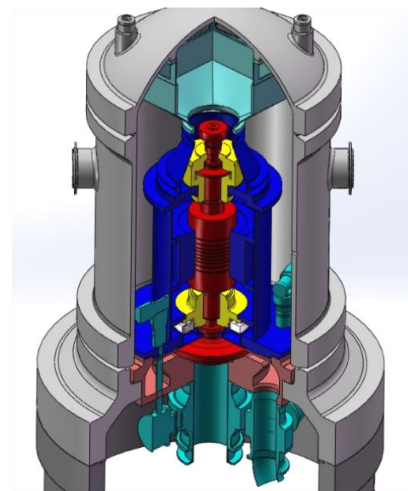


Fig. 1. The model of HTR.

Table 1: Rotor dynamics parameters

Parameters	Value	Unit
Total mass(m)	4230	kg
Centroid position	Z=1.5	m
Equatorial moment of inertia $J_x = J_y$	2690	kgm ²
Polar moment of inertia J_z	215	kgm ²
Rotor diameter at bearing (D)	0.3	m

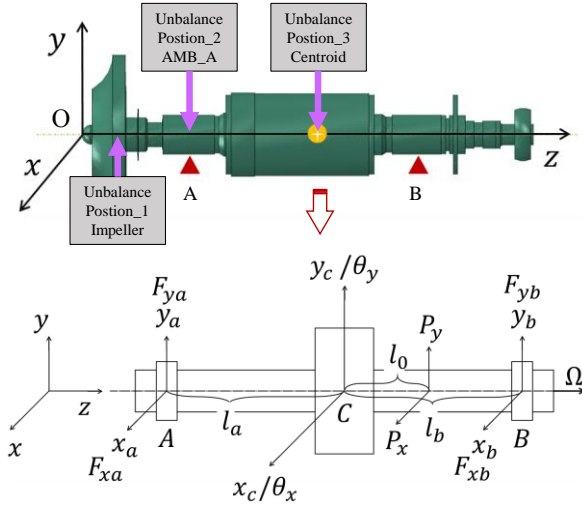


Fig. 2. The model of rigid rotor.

B. The AMB model

The design of the radial bearing is shown in Fig. 3. It is an 8-poles bearing. The design parameters of the bearing are shown in Table 2.

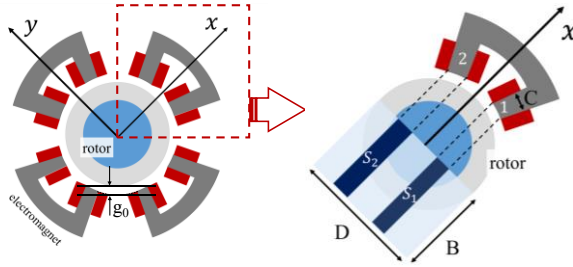


Fig. 3. The model of AMB.

Table 2: Design parameters of AMBs

Parameters	Value	Unit
AMB-A position	Z=0.8	m
AMB-B position	Z=2.6	m
AMB-A arm(l_a)	0.7	m
AMB-A arm(l_b)	1.1	m
Magnetic permeability(μ_0)	$4\pi/10^7$	H/m
Number of coil turns(N)	30	-
Bearing thickness(B)	0.3	m
Single pole width(C)	0.06	m
Bias current(I_0)	20	A
AMB Gap (g_0)	0.001	m
Pole projected area $S_1=S_2$	0.243	m^2
Bearing projected area A_j	0.09	m^2
Radio of projected area r_p	0.37	-

In Fig. 3, the notations S_1 and S_2 represent the projected area of the magnetic pole 1 and the magnetic pole 2 on the rotor in the y-plane. The notation A_j represent the projected area of the magnetic bearing on

the rotor in the y-plane, $A_j = B \times D$, and the notation r_p is the ratio of the projected area of magnetic pole to the projected area of the bearing, where $r_p = \frac{S_1+S_2}{B \times D}$.

C. Rotor unbalanced load

In the ISO 1940-1 standard [1], there is a double logarithmic linear relationship between the maximum permissible radial imbalance e_{per} (g.mm/kg) and the maximum rotation speed n_{max} (r/min) for the same unbalance level:

$$\log_{10}(e_{per}) = A \times \log_{10}(n_{max}) + B.$$

According to the ISO1940-1 standard, the unbalanced level of the rotor is G6.3. The relationship between the radial unbalance and the maximum rotation speed is as follows:

$$\log_{10}(e_{per}) = -\log_{10}(n_{max}) + 4.778,$$

i.e.,

$$e_{per} = \frac{10^{4.778}}{n_{max}} = \frac{6281 \times 10^{-6}}{\Omega_{max}} (\text{kg} \cdot \text{m}),$$

where Ω_{max} is angular speed(rad/s). Through rotor mass of $m=4230\text{kg}$, the unbalance U can be obtained:

$$U = e_{per} \times m = \frac{26.569}{\Omega_{max}} (\text{kg} \cdot \text{m}).$$

According to the centrifugal force equation $F_p = m\Omega^2 r$, the centrifugal force produced by the rotor at this unbalanced amount is as:

$$F_p = U \times \Omega^2 = \frac{26.57\Omega^2}{\Omega_{max}} (\text{N}).$$

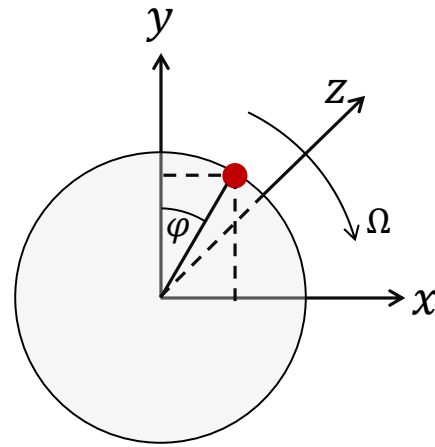


Fig. 4. Rotor initial phase angle.

The initial phase angle of the unbalanced mass of the rotor is defined in Fig. 4. The components of the centrifugal force in the x and y directions can be obtained [2]:

$$\begin{aligned} P_x &= F_p \sin(\Omega t + \varphi), \\ P_y &= F_p \cos(\Omega t + \varphi). \end{aligned}$$

In the three typical unbalanced positions in Fig. 2, unbalances are respectively set to analyze the effects of

unbalances at different positions on the rotor response results. Specific unbalanced arms are shown in Table 3.

Table 3: Design parameters of AMBs

Unbalance Position Number	Arm	Unit
UBP1:Impeller position (l_{01})	-1.2	m
UBP2:AMB-A position (l_{02})	-0.7	m
UBP3:Centroid position(l_{03})	0	m

II. COUPLING DYNAMIC AND CONTROL METHODS

A. Rotor dynamic equation

The radial load of the rotor is perpendicular to the rotational speed, so a change of radial load produces a gyroscopic moment, resulting in the four degrees of freedom of the two radial bearings being coupled together. Therefore, the four degrees of freedom of the two radial bearings need to be analyzed together. The axial load is parallel to the rotational speed, so the change of the axial load does not produce a gyroscopic moment and can be analyzed separately. The analysis of axial bearing is similar to radial bearings, but with less freedom and simple analysis, which is not described.

According to Fig. 2 to establish the rotor dynamics equation, the first is the rotor force balance equation:

$$m\ddot{x}_c = F_{xa} + F_{xb} + P_x, \quad (1)$$

$$m\ddot{y}_c = F_{ya} + F_{yb} + P_y. \quad (2)$$

Secondly, the torque balance equation of the rotor is considered, considering the gyroscopic effect of the rotor:

$$J_x\ddot{\theta}_x - J_z\Omega\dot{\theta}_y = -F_{ya}l_a + F_{yb}l_b + P_y l_0, \quad (3)$$

$$J_y\ddot{\theta}_y + J_z\Omega\dot{\theta}_x = F_{xa}l_a - F_{xb}l_b - P_x l_0. \quad (4)$$

Combining equations 1-4 and representing them with a matrix equation:

$$M\ddot{X}_c + C\dot{X}_c = T_f F + P. \quad (5)$$

Where,

$$M = \begin{bmatrix} m & & & \\ & m & & \\ & & J_x & \\ & & & J_y \end{bmatrix},$$

$$C = \begin{bmatrix} 0 & & & \\ & 0 & & \\ & & 0 & -J_z\Omega \\ & & J_z\Omega & 0 \end{bmatrix},$$

$$T_f = \begin{bmatrix} 1 & 1 & 0 & 0 \\ 0 & 0 & 1 & 1 \\ 0 & 0 & -l_a & l_b \\ l_a & -l_b & 0 & 0 \end{bmatrix},$$

$$F = \begin{bmatrix} F_{xa} \\ F_{xb} \\ F_{ya} \\ F_{yb} \end{bmatrix}; P = \begin{bmatrix} P_x \\ P_y \\ P_y l_0 \\ -P_x l_0 \end{bmatrix}; X_c = \begin{bmatrix} x_c \\ y_c \\ \theta_x \\ \theta_y \end{bmatrix}.$$

The displacement and the rotation angle of the

centroid are transformed into displacements in the four directions of AMB-A and AMB-B by the transformation matrix T_t , i.e., $X_c = T_t X$, where,

$$X = \begin{bmatrix} x_a \\ x_b \\ y_a \\ y_b \end{bmatrix},$$

$$T_t = \begin{bmatrix} \frac{l_b}{l_a+l_b} & \frac{l_a}{l_a+l_b} & 0 & 0 \\ 0 & 0 & \frac{l_b}{l_a+l_b} & \frac{l_a}{l_a+l_b} \\ 0 & 0 & -\frac{1}{l_a+l_b} & \frac{1}{l_a+l_b} \\ \frac{1}{l_a+l_b} & -\frac{1}{l_a+l_b} & 0 & 0 \end{bmatrix}.$$

Equation 5 is converted to equation 6 by $X_c = T_t X$:

$$MT_t\ddot{X} + CT_t\dot{X} = T_f F + P. \quad (6)$$

B. The relationship between AMB force and rotor displacement under PD control

The equation for the electromagnetic force generated by a single electromagnet is:

$$F_{magnetic} = \frac{\mu_0 N^2 I^2 A_j r_p}{8g^2} = k \frac{I^2}{g^2}. \quad (7)$$

Where $k = \frac{\mu_0 N^2 A_j r_p}{8}$, the notation g is the gap between the AMB and the rotor as shown in Fig. 3, the notation I is the current of the AMB [3].

Take the relationship between F_{xa} and x_a as an example to derive the relationship between electromagnetic force and displacement in each direction. Assume that the initial gap of the bearing is g_0 , then the gap of the bearing after the rotor moves is:

$$\begin{cases} g_{xa+} = g_0 - x_a \\ g_{xa-} = g_0 + x_a \end{cases}. \quad (8)$$

Where the notation g_{xa+} is the gap between the rotor and the magnetic poles of bearing A in x positive direction. The notation g_{xa-} is the gap between the rotor and the magnetic poles of bearing A in x reverse direction.

Two magnetic poles symmetrical at the x_a direction use differential control, i.e.:

$$\begin{cases} I_{xa+} = I_0 + I_{xa} \\ I_{xa-} = I_0 - I_{xa} \end{cases}. \quad (9)$$

Where the notation I_{xa+} is the control current of the magnetic poles of bearing A in x positive direction and the notation I_{xa-} is the control current of the magnetic poles of bearing A in x reverse direction.

Therefore, the relationship between bearing force and displacement is as follows:

$$F_{xa} = k \left[\frac{(I_0 + I_{xa})^2}{(g_0 - x_a)^2} - \frac{(I_0 - I_{xa})^2}{(g_0 + x_a)^2} \right]. \quad (10)$$

The relationship between force and displacement and current is linearized. The two order Taylor expansion is performed at $x_a = 0$ and $I_{xa} = 0$ and the second-order and higher-order terms are ignored:

$$\left[\frac{(I_0 + I_{xa})^2}{(g_0 - x_a)^2} - \frac{(I_0 - I_{xa})^2}{(g_0 + x_a)^2} \right] \approx I_{xa} \frac{4I_0}{g_0^2} + x_a \frac{4I_0^2}{g_0^3}. \quad (11)$$

The relationship between AMB force and control current and rotor displacement at direction of x_a is obtained:

$$F_{xa} = k \left(I_{xa} \frac{4I_0}{g_0^2} + x_a \frac{4I_0^2}{g_0^3} \right). \quad (12)$$

Finally, the relationship between AMB force F and X is as follows:

$$F = k \frac{4I_0}{g_0^2} I_C + k \frac{4I_0^2}{g_0^3} X. \quad (13)$$

Where I_C is the control current:

$$I_C = \begin{bmatrix} I_{xa} \\ I_{xb} \\ I_{ya} \\ I_{yb} \end{bmatrix}.$$

PD control is adopted between control current I_C and displacement X , as shown in Fig. 5 [4]:

$$I_C = -pX - d\dot{X}, \quad (14)$$

Where,

$$p = \text{diag}[p_a, p_b, p_a, p_b], \\ d = \text{diag}[d_a, d_b, d_a, d_b].$$

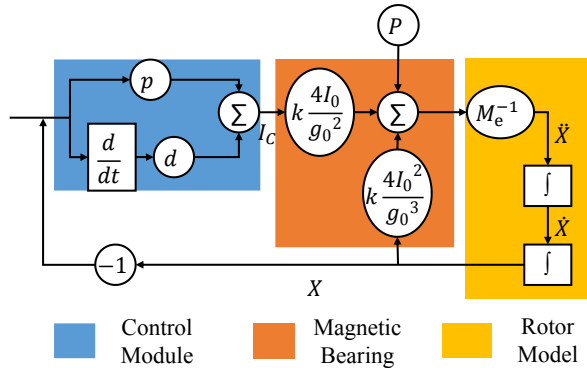


Fig. 5. the block diagram of the closed loop controlled system.

By combining equations 6, 13, and 14, the rotor dynamics equation that coupled dynamic equations and control methods are obtained:

$$M_e \ddot{X} + C_e \dot{X} + K_e X = P. \quad (15)$$

Where,

$$M_e = MT_t, \\ C_e = CT_t + k \frac{4I_0}{g_0^2} T_f d, \\ K_e = k \frac{4I_0}{g_0^2} T_f p - k \frac{4I_0^2}{g_0^3} T_f.$$

By setting the equivalent stiffness and the equivalent damping ratio to determine the control matrix p and d . Setting $K_e(1,1) = K_e(1,2) = K$, the p can be obtained and setting damping ratio is ζ , the d can be obtained through equations 16,17:

$$C_e(1,1) = 2M_e(1,1) \sqrt{\frac{K_e(1,1)}{M_e(1,1)}} \zeta, \quad (16)$$

$$C_e(1,2) = 2M_e(1,2) \sqrt{\frac{K_e(1,2)}{M_e(1,2)}} \zeta. \quad (17)$$

III. NUMERICAL SIMULATION RESULTS

A. Time response results

The numerical solution method of time domain equation mainly includes mode superposition method and direct integration method. The mode superposition method needs to first obtain the mode shape of the model, which is suitable for calculating the seismic response that discard the influence of higher-order modes. This method is limited to applications within the elastic range and takes more time to calculate. The direct integration method does not require vibration mode analysis, and the equation is directly integrated by discrete time. The general direct integration methods include linear acceleration method, Wilson- θ method and Newmark- β method. For the linear integration method, the stability condition depends on the step size, and the step size depends on the minimum period of the discrete structure, which is difficult to determine. The Wilson- θ method improves the linear integration method by introducing the θ factor, and the convergence of the method can be ensured by defining the θ . The Newmark- β method is another variant of the linear acceleration method. Compared with the Wilson- θ method, its calculation accuracy and computational stability are more controllable, but the calculation process is more complicated [5,6].

The rotor's time-domain result of unbalanced response is solved by equation 15 and Wilson- θ method. The initial condition of the rotor at time 0 s is $\dot{X}(0) = \dot{X}_0$, $X(0) = X_0$. \dot{X}_0 can be solved by \dot{X}_0 , X_0 and equation 15 as $\dot{X}_0 = M_e^{-1}(P_0 - K_e X_0 - C_e \dot{X}_0)$.

Dissipate the entire analysis time into multiple Δt , and assume that the acceleration in each $\theta \Delta t$ period changes linearly, where θ is time magnification factor, that is shown in Fig. 6.

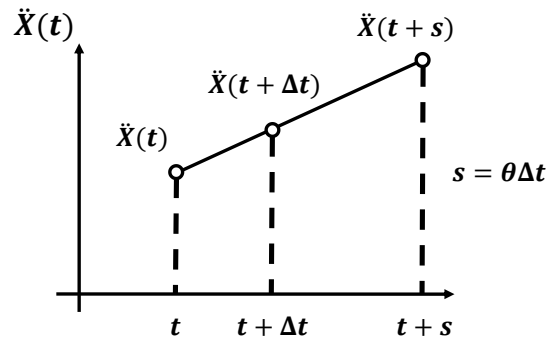


Fig. 6. Linear change of acceleration.

Set,

$$\Delta \ddot{X}_S(t) = \ddot{X}(t+s) - \ddot{X}(t), \quad (18)$$

define the function of \ddot{X} about τ ,

$$\ddot{X}(t + \tau) = \ddot{X}(t) + \frac{\tau}{s} \Delta \ddot{X}_s(t). \quad (19)$$

Perform one and two integrals for τ and take $\tau=s$:

$$\dot{X}(t + s) = \dot{X}(t) + s\ddot{X}(t) + \frac{s}{2} \Delta \ddot{X}_s(t), \quad (20)$$

$$\begin{aligned} X(t + s) &= \\ X(t) + s\dot{X}(t) + \frac{s^2}{2} \ddot{X}(t) + \frac{s^2}{6} \Delta \ddot{X}_s(t). \end{aligned} \quad (21)$$

Bring equation 18 into equations 20 and 21:

$$\begin{aligned} \dot{X}(t + s) &= \\ \dot{X}(t) + \frac{s}{2} \ddot{X}(t) + \frac{s}{2} \ddot{X}(t + s), \end{aligned} \quad (22)$$

$$\begin{aligned} X(t + s) &= \\ X(t) + s\dot{X}(t) + \frac{s^2}{6} [\ddot{X}(t + s) + 2\ddot{X}(t)]. \end{aligned} \quad (23)$$

At $t+s$, the equation of motion of the rotor is:

$$\begin{aligned} M_e \ddot{X}(t + s) + C_e \dot{X}(t + s) + K_e X(t + s) \\ = P(t + s). \end{aligned} \quad (24)$$

Combining equations 22, 23, and 24 and eliminating $\dot{X}(t + s)$ and $\ddot{X}(t + s)$:

$$\begin{aligned} \left(\frac{6M_e}{s^2} + \frac{3C_e}{s} + K_e \right) X(t + s) = \\ \left[\left(\frac{6M_e}{s^2} + \frac{3C_e}{s} \right) X(t) + \left(\frac{6M_e}{s} + 2C_e \right) \dot{X}(t) \right. \\ \left. + \left(2M_e + \frac{sC_e}{2} \right) \ddot{X}(t) + P(t + s) \right]. \end{aligned} \quad (25)$$

Equation 26 can be obtained from Fig. 6:

$$\ddot{X}(t + s) = \theta \ddot{X}(t + \Delta t) + (1 - \theta) \ddot{X}(t). \quad (26)$$

Substitute equation 26 into equation 23, and set $s = \theta \Delta t$:

$$\begin{aligned} \ddot{X}(t + \Delta t) &= \frac{6}{\theta^3 \Delta t^2} [X(t + s) - X(t)] \\ &\quad - \frac{6}{\theta^2 \Delta t} \dot{X}(t) + \left(1 - \frac{3}{\theta} \right) \ddot{X}(t). \end{aligned} \quad (27)$$

In equation 22 and equation 23, set $s = \theta \Delta t$:

$$\begin{aligned} \dot{X}(t + \Delta t) &= \\ \dot{X}(t) + \frac{\Delta t}{2} \ddot{X}(t) + \frac{\Delta t}{2} \ddot{X}(t + \Delta t), \end{aligned} \quad (28)$$

$$X(t + \Delta t) =$$

$$X(t) + \Delta t \dot{X}(t) + \frac{\Delta t^2}{6} [\ddot{X}(t + \Delta t) + 2\ddot{X}(t)]. \quad (29)$$

The entire iterative solution process is as follow five steps:

Step1: $X(t + s)$ is solved by $X(t)$, $\dot{X}(t)$, $\ddot{X}(t)$, $P(t + s)$ and equation 25;

Step2: $\ddot{X}(t + \Delta t)$ is solved by $X(t)$, $\dot{X}(t)$, $\ddot{X}(t)$, $X(t + s)$ and equation 27;

Step3: $\dot{X}(t + \Delta t)$ is solved by $\dot{X}(t)$, $\ddot{X}(t)$, $\ddot{X}(t + \Delta t)$ and equation 28;

Step4: $X(t + \Delta t)$ is solved by $X(t)$, $\dot{X}(t)$, $\ddot{X}(t)$, $\ddot{X}(t + \Delta t)$ and equation 29;

Step5: Replace t with $t + \Delta t$, repeat step1 to step4.

For the wilson $-\theta$ method, the calculation is stable when $\theta > 1.37$, generally taking $\theta = 1.4$ [6].

When the rotation speed is 4000 r/min and the unbalanced position is UBP1. The K is 1×10^7 N/m and the damping ratio is 0.5. The time-domain response results of rotor displacement and AMB force within 0.2 s are shown in Fig. 7 and Fig. 8.

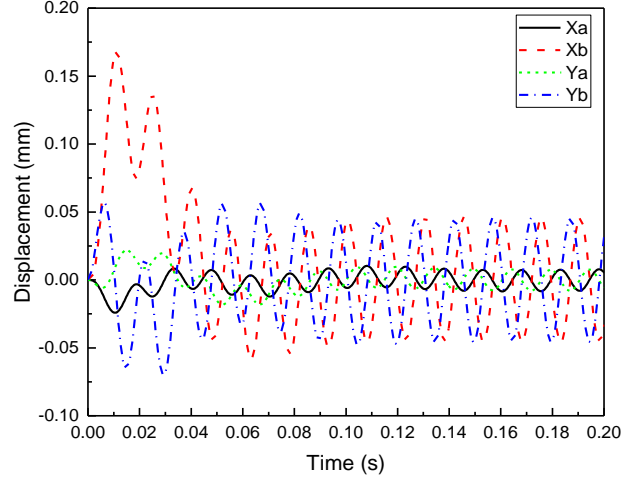


Fig. 7. Time-domain response results of rotor displacement (4000r/min).

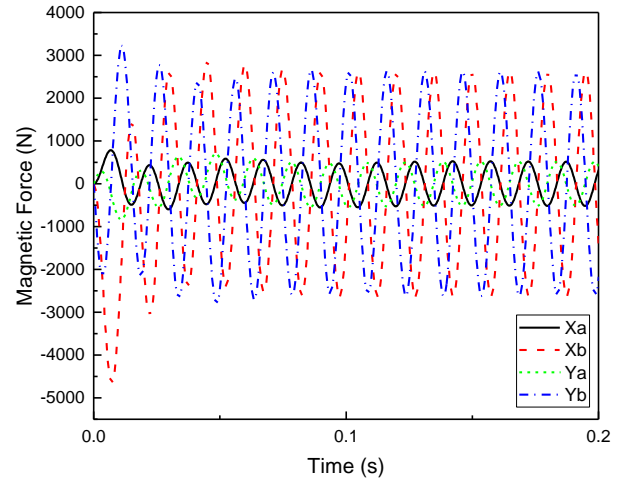


Fig. 8. Time-domain response results of AMB force (4000r/min).

B. The effect of unbalanced position on the response result

In order to analyze the rotor displacement response and bearing load response during the entire speed-up process (from 0r/min to 4000r/min), the 81 time-domain response curves of the rotor is calculated at intervals of 50r/min. A Fourier transform is performed on each time-domain response curve to obtain a frequency-domain curve of the rotor at a fixed rotational speed (the Fig. 9 and the Fig. 10 show the frequency-domain curve, which is obtained through Fourier transform from Fig. 7 and Fig. 8). The 81 frequency-domain curves are drawn together, and the envelope curves of 81 curves are the frequency-domain curves during the rotor speed-up process, and the peaks of Fig. 9 and Fig. 10 are indicated by red circles in Figs. 9-16 [7].

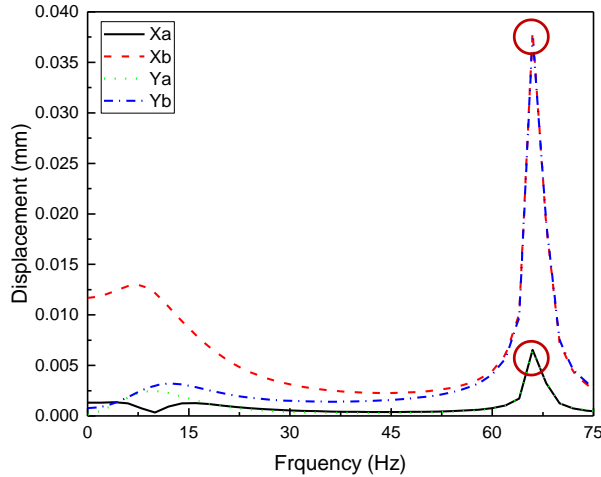


Fig. 9. Frequency-domain response results of rotor displacement (4000r/min).

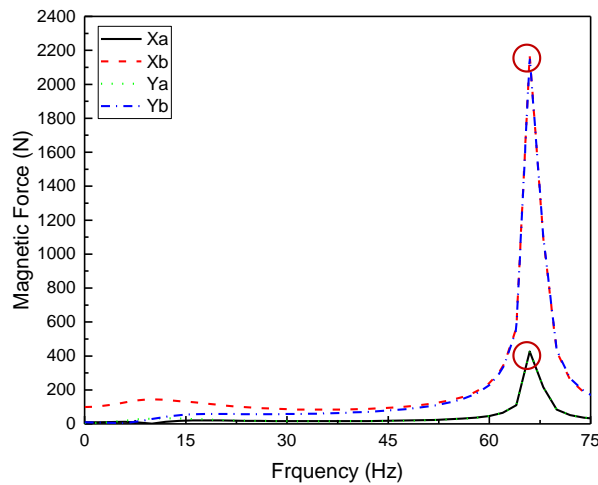


Fig. 10. Frequency-domain response results of AMB force (4000r/min).

The AMB stiffness is $K = 1 \times 10^7$ N/m and the damping ratio is $\zeta = 0.5$. The frequency-domain effect of the unbalance position (UBP) on the rotor displacement and AMB force is analyzed, which is shown in Fig. 11 and Fig. 12.

From Fig. 11 and Fig. 12, it can be seen that when the stiffness and damping ratio are the same, the farther the unbalance mass deviates from the centroid of the rotor, the greater the displacement of rotor and force of AMB. Compared with AMB-A and AMB-B, it can be found that for the condition of UBP1 and UBP2, because the position of AMB-B is farther from the unbalanced load than the position of AMB-A, this means that its arm is longer and the bearing force it needs to bear is greater, and its displacement response is also more pronounced.

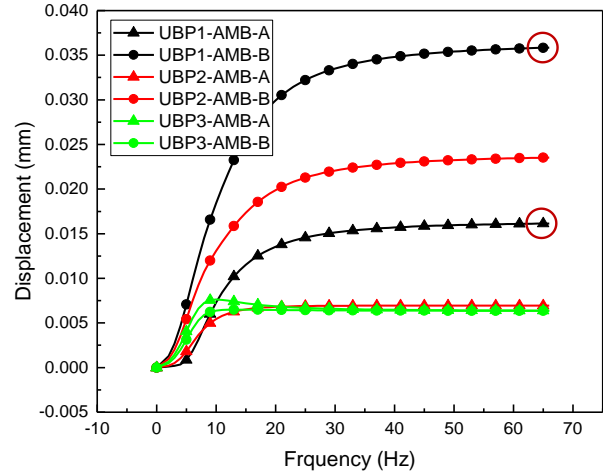


Fig. 11. Rotor displacement frequency response curve (different unbalance position).

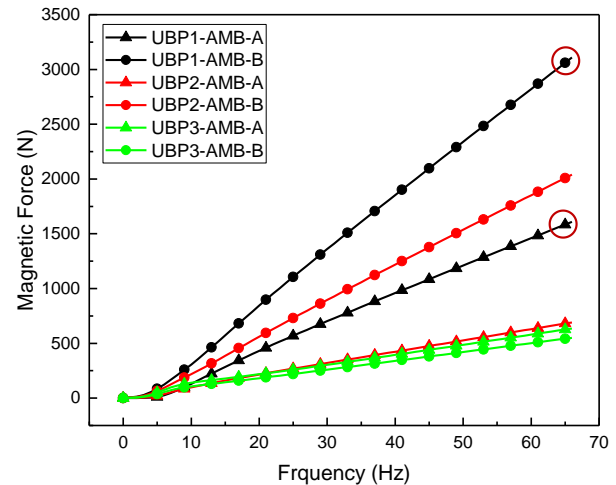


Fig. 12. AMB force frequency-domain curve (different unbalance position).

C. The effect of AMB stiffness on the response result

Select the unbalance condition UBP1 with maximum rotor displacement and bearing load according to section B and fix damping ratio $\zeta = 0.5$ to analyze the frequency-domain effect of different bearing stiffness on rotor displacement and AMB force. The results are shown in Fig. 13 and Fig. 14.

From Fig. 13 and Fig. 14, it can be seen that as the stiffness increases, the rotor displacement decreases and the AMB force increases, but the reduction of the rotor displacement is not obvious and the increase of the AMB force is significant which may lead to saturation of the magnetic actuator. [8] By selecting an appropriate bearing stiffness, both rotor displacement and bearing load can be guaranteed.

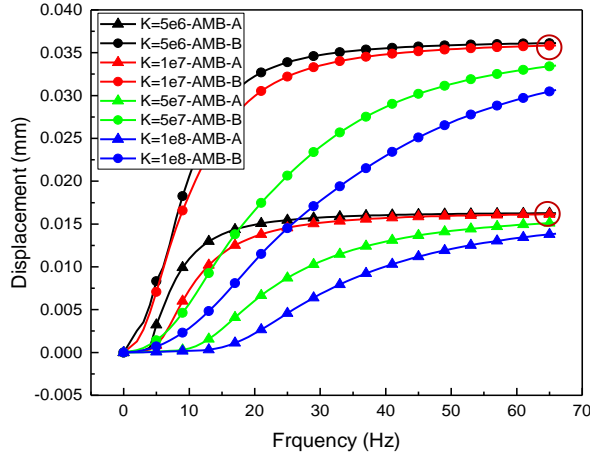


Fig. 13. Rotor displacement frequency response curve.

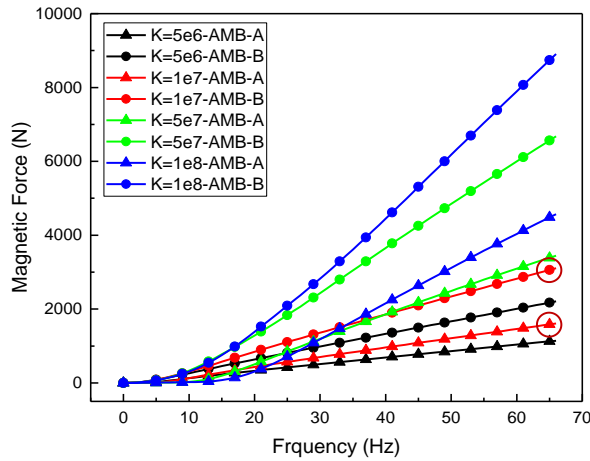


Fig. 14. AMB force frequency response curve.

D. The effect of damping ratio on the response result

The unbalance condition is same as section C, and fix stiffness $K = 1 \times 10^7 \text{N/m}$ to analyze the effect of different stiffness ratio on rotor displacement and AMB force. The results are shown in Fig. 15 and Fig. 16.

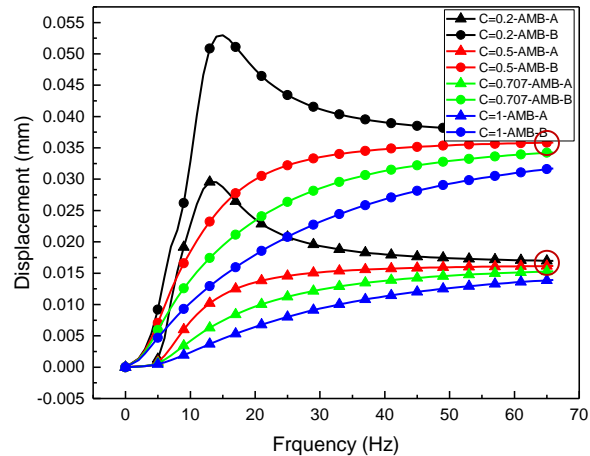


Fig. 15. Rotor displacement frequency response curve.

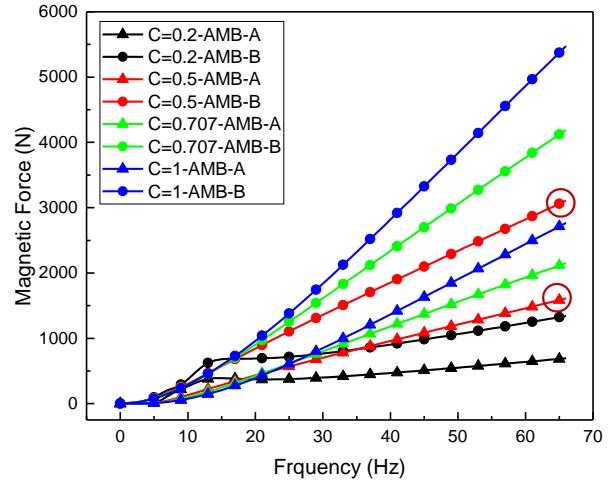


Fig. 16. AMB force frequency response curve.

From Figs. 15 and 16, it can be seen that the results are similar to Section C. As the damping ratio increases, the rotor displacement decreases and the AMB force increases. By selecting appropriate load damping ratio, both rotor displacement and bearing load can be guaranteed.

IV. CONCLUSION

When the stiffness and damping ratio are the same, the farther the unbalance mass deviates from the centroid of the rotor, the greater the displacement of rotor and force of AMB. The arm from the bearing to the unbalance position is longer and the bearing force it needs to bear is greater, and its displacement response is also more pronounced.

Increasing the stiffness and damping ratio of bearings can effectively reduce the unbalance response of the rotor, but it will significantly increase the bearing load. Therefore, when determining the bearing stiffness and damping ratio, it is necessary to consider the bearing load and displacement comprehensively and select the optimal solution.

The follow-up work of this paper mainly includes: 1) Using the method of this paper to calculate the unbalanced response of the system under different conditions, and compare it with the actual running data to realize the correction of the system model. This work can be combined with the linear identification method [9]. 2) When a rotor-drop occurs, the system may exhibit nonlinearity [10-12], and it is necessary to consider extending the work of this paper to a nonlinear model.

ACKNOWLEDGMENT

This paper is financially supported by the National Science and Technology Major Project of China (2011ZX069) and Project 61305065 supported by NSFC.

REFERENCES

[1] ISO Standard 1940, "Balance Quality of Rotating

- Rigid Bodies,” *International Organization for Standardization ISO*, 1973.
- [2] J. Yu and C. Zhu, “A multi-frequency disturbances identification and suppression method for self-sensing AMB rotor system,” *[J]. IEEE Transactions on Industrial Electronics*, p. (99):1-1, 2017.
- [3] G. Schweitzer and E. H. Maslen, “Magnetic bearings: Theory, design, and application to rotating machinery,” 2009.
- [4] R. Herzog, P. Bühler, C. Gähler, and R. Larssonneur, “Unbalance compensation using generalized notch filters in the multivariable feedback of magnetic bearings,” *IEEE Trans. Control Sys. Tech.*, vol. 4, no. 5, pp. 580-586, 1996.
- [5] I. Gladwell and R. Thomas, “Stability properties of the Newmark, Houbolt and Wilson θ methods,” *International Journal for Numerical and Analytical Methods in Geomechanics*, vol. 4, no. 2, pp. 143-158, 1980.
- [6] L. Aiqun and D. Youliang, *Aseismic Analysis of Engineering Structures* [M]. High Education Press, 2010.
- [7] C. R. Burrows and M. N. Sahinkaya, “Vibration control of multi-mode rotor bearing systems,” *In Proceedings of the Royal Society of London (Series A)*, vol. 386, 1983.
- [8] B. Shafai, S. Beale, P. Larocca, et al., Magnetic bearing control systems and adaptive forced balancing, *[J]. Control Systems IEEE*, vol. 14, no. 2, pp. 4-13, 1994.
- [9] Z. Sun, Y. He, J. Zhao, Z. Shi, L. Zhao, and S. Yu, “Identification of active magnetic bearing system with a flexible rotor,” *Mechanical Systems & Signal Processing*, vol. 49, no. 1-2, pp. 302-316, 2014.
- [10] Z. Sun, J. Zhao, Z. Shi, et al., “Soft sensing of magnetic bearing system based on support vector regression and extended Kalman filter,” *[J]. Mechatronics*, vol. 24, no. 3, pp. 186-197, 2014.
- [11] Z. Sun, X. Yan, J. Zhao, et al., “Dynamic behavior analysis of touchdown process in active magnetic bearing system based on a machine learning method,” *[J]. Science & Technology of Nuclear Installations*, 2017 (5):1-11, 2017.
- [12] C. A. Fonseca, I. F. Santos, and H. I. Weber, “Influence of unbalance levels on nonlinear dynamics of a rotor-backup rolling bearing system,” *[J]. Journal of Sound & Vibration*, 394:482-496, 2017.



Guowei Du graduated from School of Aerospace, and now is a fifth year Ph.D. candidate at the Institute of Nuclear and New Energy Technology of Tsinghua University. His main research direction is rotor dynamics and active magnetic bearing control.



Zhe Sun is currently an Associate Professor and Ph.D. Supervisor of Tsinghua University. His research interests are control and monitoring of active magnetic levitation system, rotor dynamics, statistical learning theory and its engineering application, etc.